



Universidade do Minho
Escola de Engenharia

Semana da Escola de Engenharia October 24 - 27, 2011

ON THE EFFECT OF THE WALL SLIP BOUNDARY CONDITON

Luis L. Ferrás¹, J. Miguel Nóbrega¹, Fernando T. Pinho² and Olga S. Carneiro¹

¹IPC/I3N – Institute for Polymers and Composites, University of Minho, Campus de Azurém,
4800-058 Guimarães, Portugal

²Centro de Estudos de Fenómenos de Transporte, Faculdade de Engenharia da Universidade do Porto, Rua Dr. Roberto Frias s/n, 4200-465 Porto, Portugal

KEYWORDS

Flow Modelling, Slip boundary condition, non-Newtonian fluids, Finite volume method.

ABSTRACT

This work describes the implementation and assessment of the wall slip boundary condition in a 3D numerical modelling code, based on the finite volume method, that is being developed by the research team. Several phenomenological models relating the velocity and the shear stress at the wall were implemented. The capabilities of the new numerical code are illustrated with three case studies where the wall slip boundary conditions play an important role, namely the flow in a smooth contraction, the stick-slip phenomenon an the flow in a profile extrusion die. The results obtained are qualitatively in accordance with the theoretical expectations and evidence the importance of wall slip.

INTRODUCTION

Wall slip of polymer melts has been studied by several authors (Mitsoulis et al. 2005, Hatzikiriakos et al. 1993, Potente et al. 2002), resulting in the development of phenomenological models to handle the problem. Since this subject is still under study, a general slip model that works for every polymer/metal interface materials is still missing. The major difficulty is the dependence of the slip velocity on a series of variables, namely, the interaction between the liquid and the solid, the surface roughness, the shear rate and the molecular weight of the polymer. The existence of slip is evidenced in plots of pressure drop versus flow rate and thickness dependences, by the existence of a shear rate threshold and by the occurrence of extrusion defects. A direct characterization of the flow velocity at the interface can be obtained by tracer particles and near filed laser velocimetry. Even with these techniques the physics is

not completely revealed demanding further investigations to better understand the phenomena involved in wall slip, for which numerical modelling can be a valuable tool.

During the last decades, the progressive development of computational fluid dynamics and of computer technology (enabling the implementation of more realistic complex rheological models together with more accurate discretization and interpolation schemes) established numerical modelling as a useful design aid, leading to significant savings in time, human and material resources. When modelling the flow of fluids, the traditional boundary condition employed at the wall is the no-slip boundary condition (Oliveira et al. 1998). However when dealing with materials that promote a non-nill velocity at the wall, for accuracy purposes the wall slip phenomenon should be considered.

This research team has been involved during the last decade on the development of computational tools to aid the design of polymer processing tools (Nóbrega et al. 2004b), which encompasses the numerical solution of flow and heat transfer equations by a finite-volume based three-dimensional code. In a first stage, the no-slip boundary condition at the flow channel walls was assumed. In fact, the majority of studies concerning the flow in extruders, extrusion dies and rheometers normally proceed from the assumption that the flowing melt adheres to the wall. However, there are certain plastic melts such as poly(vinyl chloride) (PVC), high-density polyethylene (HDPE), polypropylene (PP) and elastomers, often used in the production of plastic profiles, that show *wall-slipping* under certain conditions (Hatzikiriakos 1993). Since wall slip within processing tool affects the overall velocity field and thus the process behaviour, it was decided to implement the wall-slip boundary condition in the above referred numerical code.

The next three sections describe the numerical code developed, including the new boundary condition



Semana da Escola de Engenharia October 24 - 27, 2011

implemented, followed by a section where its assessment is reported. The subsequent sections describe three case studies that illustrate the relevance of the new boundary condition implemented. The papers ends with the conclusions.

GOVERNING EQUATIONS

The flow of fluids is usually governed by the well-known incompressible Navier-Stokes equations (Eq. 1, 2 and 3) with the no-slip boundary condition (Navier 1822):

$$\nabla \mathbf{u} = 0 \quad (1)$$

$$\frac{\partial \rho \mathbf{u}}{\partial t} + \text{div}(\rho \mathbf{u} \otimes \mathbf{u}) = -\nabla p + \text{div}[\boldsymbol{\tau}] \quad (2)$$

$$\mathbf{u} = 0 \quad \text{in } \partial\Omega \quad (3)$$

Where \otimes is the first order tensorial product, known as the dyadic product, \mathbf{u} is the velocity vector, p is the pressure, $[\boldsymbol{\tau}]$ is the deviatoric stress tensor, Ω is a simply-connected domain in R^3 , $\partial\Omega$ is its boundary and \mathbf{n} a vector normal to $\partial\Omega$.

The stress tensor can obey the following law for generalized Newtonian fluids

$$[\boldsymbol{\tau}] = 2\eta(\dot{\gamma})[D] \quad (4)$$

with $[D]$ given by

$$[D] = \frac{1}{2}([\nabla \mathbf{u}] + [\nabla \mathbf{u}]^T) \quad (5)$$

or any other differential constitutive equations (for non-Newtonian fluids), e.g. the simplified Phan-Tien Tanner (sPTT) (Phan-Tien and Tanner 1977) model, for which the stress tensor evolution is governed by:

$$f(\text{tr}[\boldsymbol{\tau}])\boldsymbol{\tau} + \lambda \overset{\nabla}{\boldsymbol{\tau}} = \eta(\nabla \mathbf{u} + (\nabla \mathbf{u})^T) \quad (6)$$

where $f(\text{tr}[\boldsymbol{\tau}])$ is a function depending on the trace of the stress tensor, λ is the relaxation time, η is the viscosity coefficient and $\overset{\nabla}{\boldsymbol{\tau}}$ stands for Oldroyd's upper convective derivative (Eq. 7),

$$\overset{\nabla}{\boldsymbol{\tau}} = \frac{\partial \boldsymbol{\tau}}{\partial t} + \mathbf{u} \cdot \nabla \boldsymbol{\tau} - [(\nabla \mathbf{u})^T \cdot \boldsymbol{\tau} + \boldsymbol{\tau} \cdot \nabla \mathbf{u}] \quad (7)$$

The linearized function $f(\text{tr}[\boldsymbol{\tau}])$ is given by

$$f(\text{tr}[\boldsymbol{\tau}]) = 1 + \frac{\varepsilon \lambda}{\eta} \text{tr}[\boldsymbol{\tau}] \quad (8)$$

where the parameter ε is related to the elongation behaviour of the fluid. The linearized function is only acceptable for low Reynolds numbers, where small molecular deformations occur.

SLIP MODELS

In order to include the wall slip boundary condition, Eq. 3 must be replaced by any of the four slip laws that are going to be studied here: the linear (Navier 1822) and nonlinear (Schowalter 1988) Navier slip, the Hatzikiriakos (Hatzikiriakos 1993) and the asymptotic (Polyflow manual) laws.

Let $\mathbf{u} = (u_1, u_2, u_3)$ and $\boldsymbol{\tau} = (\tau_1, \tau_2, \tau_3)$ be, respectively, the velocity and stress vectors at the wall. It is required that the absolute value of the slip velocity (tangent to the boundary, subscript t) must be a function of the tangent stress vector's absolute value, as shown in Eq. 9,

$$\|\mathbf{u}_t\| = f(\|\boldsymbol{\tau}_t\|) \quad (9)$$

Here $\|\cdot\|$ stands for the usual l^2 norm and $f(\cdot): \mathbb{R} \rightarrow \mathbb{R}$ represents a general function that can be linear or nonlinear. It is also required that the vector \mathbf{u}_t should point in the direction opposite to the tangent stress $\boldsymbol{\tau}_t = (\tau_{1t}, \tau_{2t}, \tau_{3t})$, as illustrated in Fig. 1.

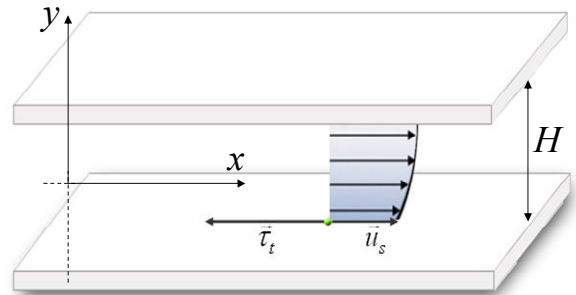


Figure 1: Schematic representation of the slip boundary condition.

The unit vector for the tangent stress $\boldsymbol{\tau}_{uni-t}$ can be easily given by



Semana da Escola de Engenharia October 24 - 27, 2011

$$\boldsymbol{\tau}_{uni-t} = \frac{1}{\|\boldsymbol{\tau}_t\|} (\tau_{1t}, \tau_{2t}, \tau_{3t}) \quad (10)$$

With little algebra it is found that the formula that verifies both requirements is given by

$$(u_1, u_2, u_3) = -f(\|\boldsymbol{\tau}_t\|) \frac{1}{\|\boldsymbol{\tau}_t\|} (\tau_{1t}, \tau_{2t}, \tau_{3t}) \quad (11)$$

For the slip models studied here, the function $f(\|\boldsymbol{\tau}_t\|)$ is set by Eq. 12a for the linear Navier slip law (Navier 1822), by Eq. 12b for the nonlinear Navier slip law (Schowalter 1988), by Eq. 12c for the Hatzikiriakos slip law (Hatzikiriakos 1993) and by Eq. 12d for the asymptotic slip law (Polyflow manual).

$$f(\|\boldsymbol{\tau}_t\|) = \begin{cases} k_l \|\boldsymbol{\tau}_t\| & (a) \\ k_{nl} (\|\boldsymbol{\tau}_t\|)^m, m \in \mathbb{R}^+ \setminus \{1\} & (b) \\ k_{H1} \sinh(k_{H2} \|\boldsymbol{\tau}_t\|) & (c) \\ k_{A1} \ln(1 + k_{A2} \|\boldsymbol{\tau}_t\|) & (d) \end{cases} \quad (12)$$

The constants $k_l, k_{nl}, k_{A1}, k_{H1}, k_{H2}, k_{A1}, k_{A2} \in \mathbb{R}^+$ are the friction coefficients for each model, which are usually obtained through the fitting of experimental observations.

WALL SLIP IMPLEMENTATION

The 3D flow fields are computed with a numerical modelling code based on the finite volume method that is being developed by the authors (Oliveira et al. 1998), (Pinho and Oliveira 2001), (Nobrega et al. 2004b). It comprises a set of routines to model the relevant physical process and uses the non-staggered hexahedral structured grid arrangement, in which all dependent variables are located at the centre of the control volumes. This greatly simplifies the adoption of general curvilinear coordinates for the mesh (Oliveira et al. 1998), being the Cartesian (x_1, x_2, x_3, t) coordinates converted into general curvilinear coordinates (ξ_1, ξ_2, ξ_3, t) that fit to the complex geometry using the following transformations,

$$\begin{aligned} x_1 &= x_1(\xi_1, \xi_2, \xi_3, t), \\ x_2 &= x_2(\xi_1, \xi_2, \xi_3, t) \\ x_3 &= x_3(\xi_1, \xi_2, \xi_3, t) \\ t &= t(t) \end{aligned} \quad (13)$$

More details on this transformation can be found in the work of (Oliveira et al. 1998). The linear momentum conservation equation written in the new coordinates is given by

$$\begin{aligned} \frac{1}{J} \frac{\partial}{\partial t} (J \rho u_i) + \frac{1}{J} \frac{\partial}{\partial \xi_j} (\rho \beta_{ij} u_i u_j) = \\ - \frac{1}{J} \frac{\partial}{\partial \xi_i} (\beta_{ii} p) + \frac{1}{J} \frac{\partial}{\partial \xi_i} (\beta_{ij} \tau_{ij}) \end{aligned} \quad (14)$$

Here, J is the Jacobian of the transformation $x_i = x_i(\xi_j)$ and β_{ij} are metric coefficients defined as the cofactor of the lj position in the Jacobian (of the coordinate change) matrix and readily interpreted as area components after integration, $i, j, k = 1, 2, 3$ are the Cartesian directions and $l = 1, 2, 3$ are the directions on the new coordinates. Notice that the velocity and stresses are assumed to be the Cartesian components.

The main modifications performed in the numerical code in order to account for slippage are related to the stress term (Eq. 15) of the linear momentum conservation equation,

$$\frac{1}{J} \frac{\partial}{\partial \xi_j} (\beta_{ij} \tau_{ij}). \quad (15)$$

After discretization, assuming hexahedral cells and applying the Gauss theorem for the i^{th} Cartesian coordinate, the diffusive term can be approximated as,

$$B_f (n_1 \tau_{i1} + n_2 \tau_{i2} + n_3 \tau_{i3})_f = B_f \tau_{if}. \quad (16)$$

where, B_f is the area of the f face and n_1, n_2, n_3 are the three Cartesian components of the unitary vector normal to the boundary. The Einstein notation is applied to f , with $f = e, w, n, s, t, b$ (the east, west, north, south, top and bottom faces).

The stress contribution is included in the source term of the algebraic discretized equation, and is given by Eq. 17,

$$S_{i-stress} = (-1)^{j-1} B_f \tau_{if}, \quad (17)$$

where $j = 0$ if $f = e, n, t$ and $j = 1$ if $f = w, s, b$.

Assuming a Couette flow near the wall, the i^{th} component of the stress vector computed at face f is given by

$$\tau_{if} = \left[\frac{\eta(\dot{\gamma})}{\delta n} \right] (u_{i,ws} - (u_{i,p})_t)_f \quad (18)$$



Semana da Escola de Engenharia October 24 - 27, 2011

where δn is the distance between the centre of the cell and the boundary face (normal to the boundary), the subscripts ws and p stand, respectively, for the boundary face (wall slip) and centre of the boundary cell, and the wall slip velocity components ($u_{i,ws}$) are given by Eq. 11.

Thus, the i^{th} boundary slip velocity vector component general formula can then be written as

$$u_{i,ws} = -f \left(\left\| \eta(\dot{\gamma}) \frac{\partial \mathbf{u}_i}{\partial \mathbf{n}} \right\| \right) \frac{\eta(\dot{\gamma}) \frac{\partial u_{i,t}}{\partial \mathbf{n}}}{\left\| \eta(\dot{\gamma}) \frac{\partial \mathbf{u}_i}{\partial \mathbf{n}} \right\|} \quad (19)$$

Depending on the boundary slip employed, the recursive calculation formula for the wall slip velocity can be rearranged to:

$$u_{i,ws} = \frac{d}{1+d} (u_{i,p})^0, \quad (20)$$

where the superscript 0 stands for a previous iteration value and the coefficient d depends on the chosen model (Ferrás et al. 2011).

The numerical problem is solved in an iterative way, as illustrated in Fig. 2.

VALIDATION

Subsequently to the numerical implementation, the numerical code was assessed through the comparison of the numerical results with the analytical solution for a Poiseuille flow between parallel plates, considering different slip conditions.

The results shown in Fig.3 allow to conclude that there is a good agreement between the numerical and the analytical results, for all the slip models implemented, thus validating the numerical implementation.

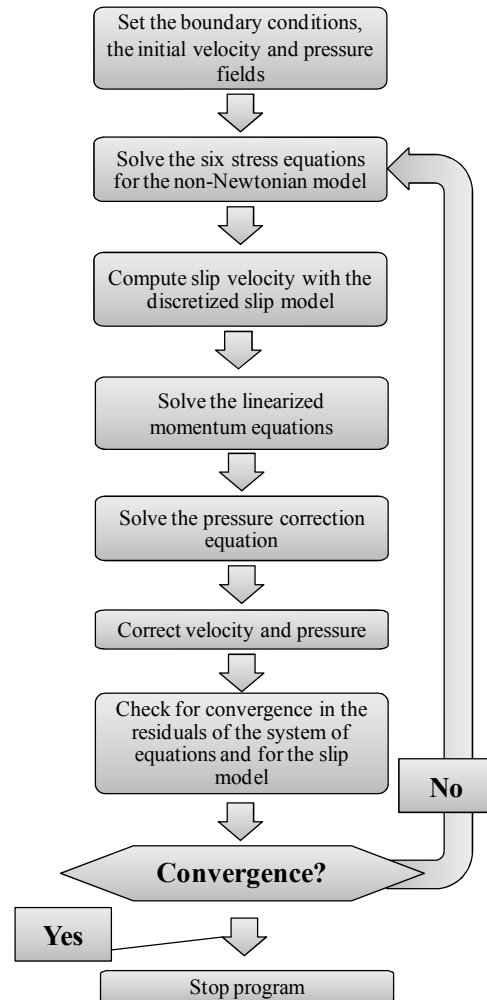


Figure 2: Iterative procedure employed on the numerical code, considering the wall slip boundary condition.



Semana da Escola de Engenharia October 24 - 27, 2011

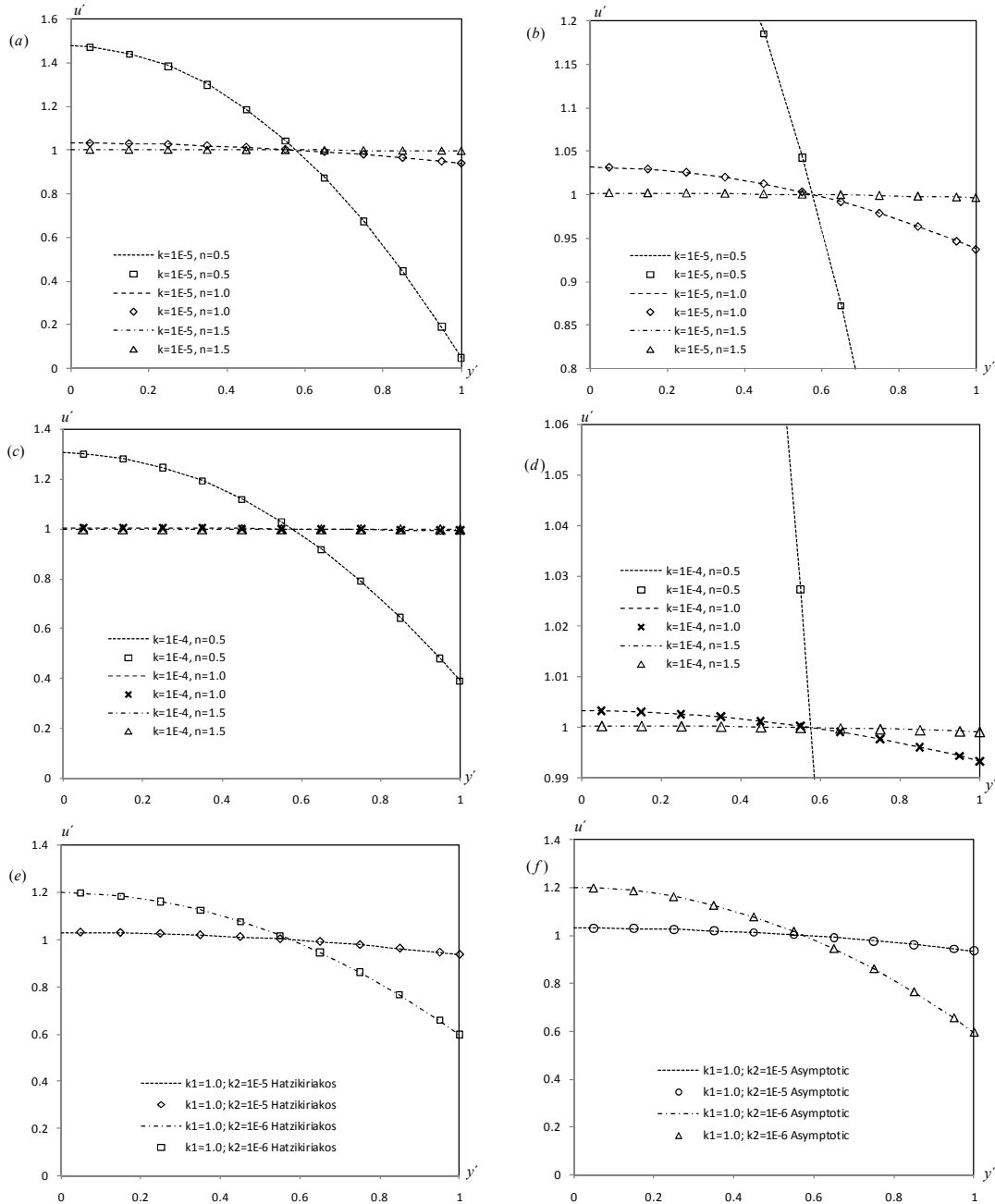


Figure 3. Comparison between analytical (lines) and numerical (symbols) solutions for a fully developed channel flow using non-linear and linear Navier slip laws with different slip coefficients $k = 1E-5$ m/Pa.s (a), $k = 1E-4$ m/Pa.s (c) and using Hatzikiriakos (e) and Asymptotic (f) slip laws. Graphs (b) and (d) show a zoomed view of graphs (a) and (c), respectively. $u' = u/U$, $y' = y/h$, where U is the imposed mean velocity and h is half the channel width.



Semana da Escola de Engenharia October 24 - 27, 2011

CASE STUDY 1

In order to assess the adequateness of the implemented boundary conditions, the numerical code was used to simulate the flow in a planar channel with variable cross-section, shown in Fig. 4, where the slip velocity at the wall was, therefore, expected to vary. The slip model used in this case study was the Non-linear Navier law (Eq. 12b). Other relevant input parameters were the following: $k_{nl} = 1E-5$; $m = 0.5$; inlet average velocity: 1.0 ms^{-1} , imposed as a rectangular (plug) velocity profile. The constitutive equation was the simplified Phan-Tien Tanner model (Eq. 6) with $Re = \rho U h / \eta = 0.001$ and a Deborah number $De = \lambda U / h = 1.0$ with $\varepsilon = 0.025$. As can be seen in Fig. 5, when slippage is taken into account, the velocity profile deviates from parabolic to plug-like.

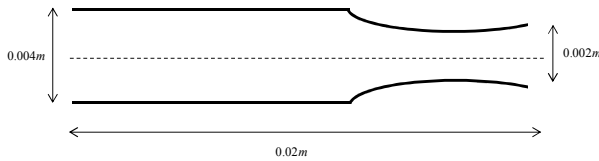


Figure 4: Geometry of the flow channel.

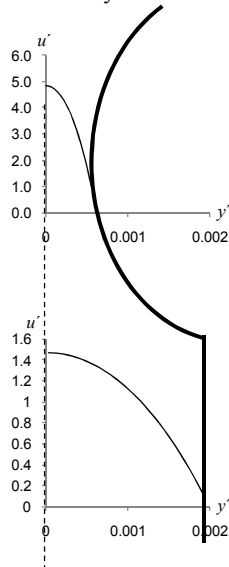


Figure 5: Velocity profiles along the axial length of the flow channel.

As shown in Figs. 5 and 6, the velocity at the wall is almost constant in the initial parallel region of the flow

channel (between locations A and B) where the velocity profile is fully developed. In the convergent region (from C to D), the melt average velocity increases and, as a consequence of an increase in the wall shear stress, there is also a progressive increase in the slip velocity. On the contrary, in the divergent zone (from D to E, exit of the channel), the opposite effect is observed. The steep decrease in the slip velocity observed in the vicinity of the transition zone (location C) can be justified by the path adopted by the melt in this region. In fact, and as expected, when an abrupt change in the geometry of the flow channel occurs, the streamlines deviate from the boundary contour of the channel, resulting in a decrease of velocity near the walls. This hypothesis can be confirmed in Fig. 7, where a streamline corresponding to the melt flowing in the vicinity of the channel walls in the transition zone is shown. As it can be seen, the distance of this line to the channel wall is higher close to the abrupt transition (location C).

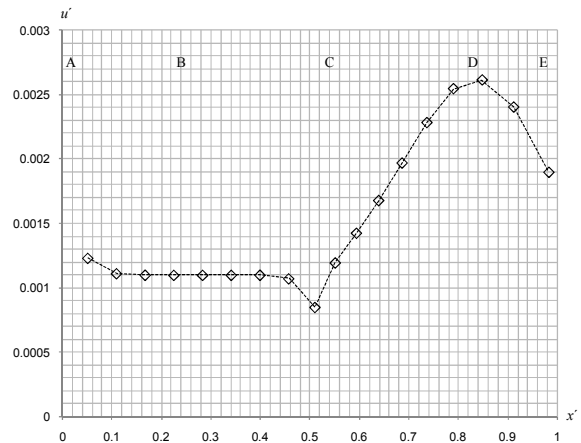
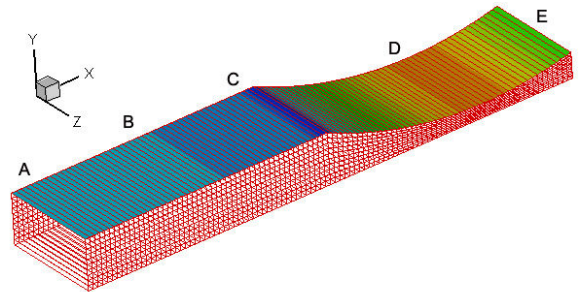


Figure 6: Slip velocities at the wall, along the axial length of the flow channel.



Universidade do Minho
Escola de Engenharia

Semana da Escola de Engenharia October 24 - 27, 2011

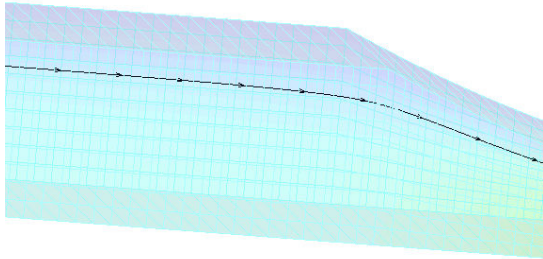


Figure 7: Streamline and mesh at the transition region (location C).

CASE STUDY 2: SLIP-STICK

The stick-slip phenomena is well-known in the polymer processing field (Hatzikiriakos 1993), being pointed out as the cause of some flow instabilities and the origin of flow defects. This case study tries to mimic the stick-slip phenomenon, modelling the flow on the domain illustrated in Fig. 8. It comprises two regions: the initial one (region I) that is delimited by two symmetry lines, and the second (region II) that is delimited by a solid wall and a symmetry line. In this way, the fluid flows freely in Region I and tends to stick to the wall in Region II, which induces the appearance of high stress fields close to the transition between regions (Oliveira et al. 1998). Obviously, the amount of slip simulated on the wall affects the level of the stresses developed. The purpose of this case study is not to study in detail the effect of slip in this particular case, but to assess qualitatively the wall slip boundary condition implemented in the numerical modelling code. So, only a limited number of slip coefficients were used and just the linear Navier slip model was employed.

The constitutive equation considered was the sPTT model and the mesh employed is illustrated in Fig. 9. It comprises 10200 cells, and is similar to the “Mesh 7” used for an analogous problem in the work of (Oliveira et al. 1998).

The tests were made for a constant Reynolds number $Re = \rho U h / \eta = 20$ and a Deborah number $De = \lambda U / h = 2.0$ with $\varepsilon = 0.025$. Six different slip intensities were tested, from no-slip ($k=0$) to the full-slip condition ($k=1$).

The convergence was achieved for all the problems studied and, as expected, it was easier to obtain for high slip velocities (high friction coefficients). This happens because the slip velocity smooths the stress singularity (Fig. 10) at the transition between regions.

The results plotted in Fig. 10 show that the amount of slip increases the velocity near the wall and in Region II and reduces the stress levels close to the transition region. This is qualitatively in accordance with the expectations.

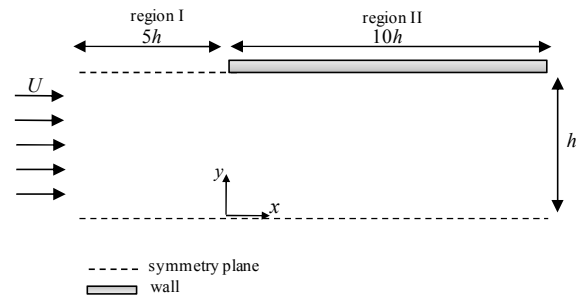


Figure 8: Schematic representation of the stick slip geometry.

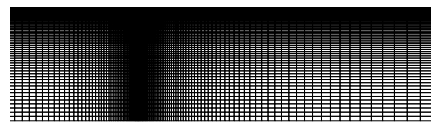


Figure 9: Mesh used in the simulation of the slip-stick flow.



Semana da Escola de Engenharia October 24 - 27, 2011

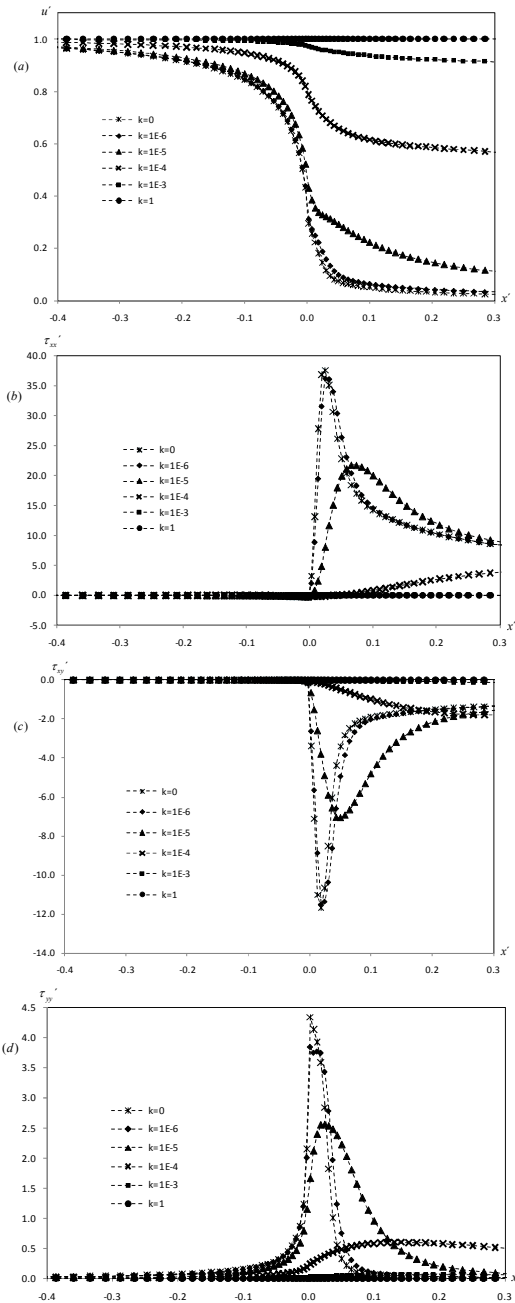


Figure 10: Distribution of (a) u' , (b) τ_{xx} , (c) τ_{xy} and (d) τ_{yy} along the slip-stick region near the wall (Note: $y/h = 0.9975$, $De = 2$, $Re = 20$, $u' = u/U$, $x' = x/h$).

CASE STUDY 3: OPTIMIZATION

As mentioned in the Introduction Section the research team has been involved in the development of numerical tools to aid the design of thermoplastic profile extrusion dies. The main problem that has to be solved by the designer when conceiving this tools is the achievement of an even flow distribution (Nobrega et al. 2004a), which is particularly difficult to attain when the cross-section of the profile to be produced comprises regions of different thicknesses, as the one illustrated in Fig. 11, mainly due to the different restrictions promoted to the flow.

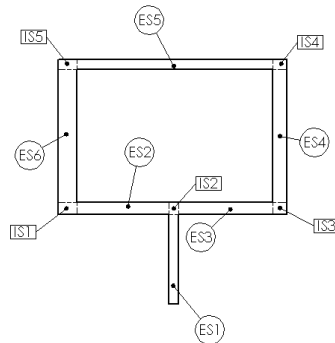


Figure 11: Cross-section of the parallel zone of the die used as case study and elemental (ES) and intersection (IS) sections considered for optimization purposes.

The automatic optimization methodology starts by the division of the profile cross-section into Elemental (ES) and Intersection (IS) Sections, that are used to monitor the flow distribution (Nobrega et al. 2004a).

The flow of the extrusion die whose cross section is illustrated in Fig. 11 was previously optimized by the numerical code, assuming the no-slip condition at the wall, obtaining the velocity distribution shown in Fig. 12(a) and 13(a) (Nobrega et al. 2004a).

The flow in the previously optimized geometry was then modelled with the new version of the flow modelling code, simulating the effect of the increase of slip at the wall. As expected, the increase of slip reduces the restriction of the wall, minimizing the effects promoted by different thicknesses, thus allowing to obtain a more balanced flow distribution, as illustrated in Fig. 12 (b,c) and 13 (b,c).



Universidade do Minho
Escola de Engenharia

Semana da Escola de Engenharia October 24 - 27, 2011

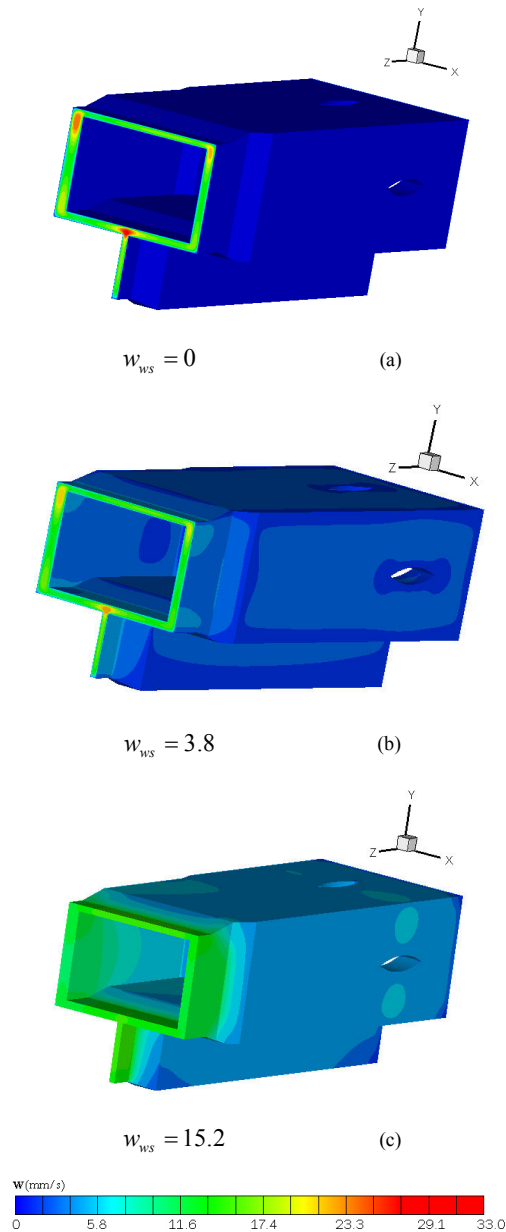


Figure 12: Velocity fields along the extrusion die channel for different levels of wall slippage: (a) $K=0$ (no slip); (b) $K=0.5E-07$; (c) $K=1.0E-06$. In this example, the average flow velocity is 15.9 mm/s and w_{ws} is the velocity (in mm/s) at a fixed point located at the final parallel zone of the flow channel.

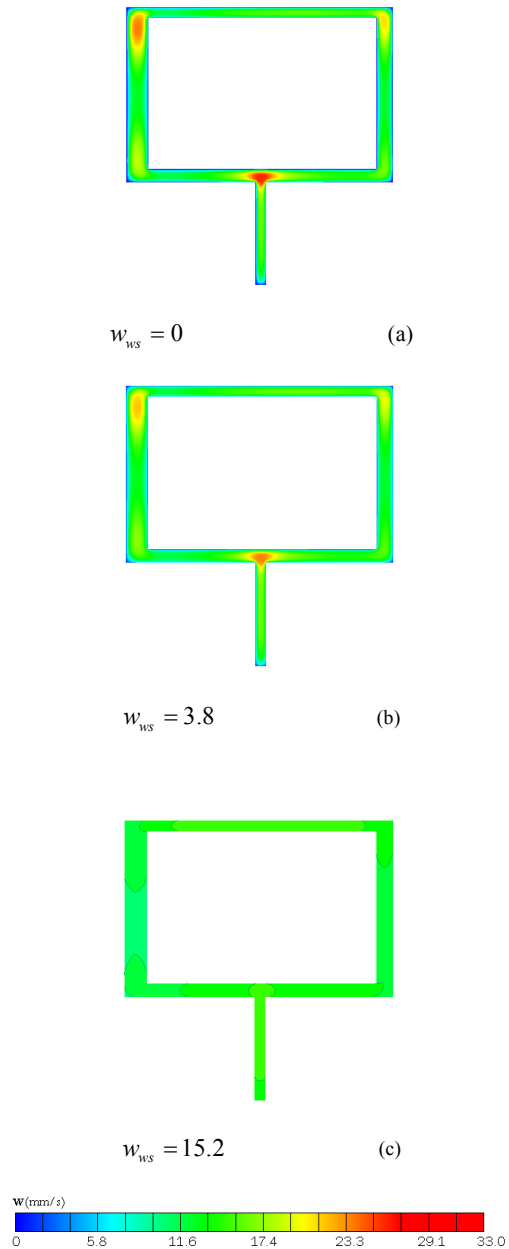


Figure 13: Velocity fields at the die exit cross-section of the extrusion die for different levels of wall slippage: (a) $K=0$ (no slip); (b) $K=0.5E-07$; (c) $K=1.0E-06$.



Universidade do Minho
Escola de Engenharia

Semana da Escola de Engenharia October 24 - 27, 2011

CONCLUSION

In this work the implementation of the slip boundary condition at the flow channel walls in a previously developed 3D numerical modelling code was described. The potential of the new numerical code was illustrated with three case studies, where the importance of wall slip was evidenced. It was also shown that the computed velocity profiles were qualitatively in accordance with the theoretical expectations, thus supporting the correctness of the numerical developments performed.

ACKNOWLEDGEMENTS

The authors would like to acknowledge the financial support provided by Fundação para a Ciência e Tecnologia under the project SFRH / BD / 37586 / 2007.

REFERENCES

- Ferrás, L.L., J.M. Nóbrega, F.T. Pinho, and O. S. Carneiro. 2011 "Implementation of Slip Boundary Conditions in the Finite Volume Method :New Techniques" (to be published).
- Hatzikiriakos S. 1993. "A Slip Model for Linear Polymers Based on Adhesive Failure." *Intern. Polymer Processing*, No. 8, 135-142.
- Mitsoulis E.; I. B. Kazatchkov; S. G. Hatzikiriakos. 2005. "The Effect of Slip on the Flow of a Branched PP Melt: Visualisation Experiments and Simulations" *Rheol Acta*, No. 44, 418-426.
- Navier C. L. M. H. 1822. "Memoire sur les lois du mouvement des fluides", *Mem. Acad. Sci. Inst. France*, No. 6, 389-440.
- Nóbrega J. M.; O. S. Carneiro; F. T. Pinho and P. J. Oliveira. 2004a. "Flow Balancing in Extrusion Dies for Thermoplastic Profiles. Part III: Experimental Assessment" *International Polymer Processing*, No. 19, 225-235.
- Nóbrega, J. M., F.T. Pinho, Oliveira P. J. and O. S. Carneiro. 2004b. "Accounting for temperature-dependent properties in viscoelastic duct flows" *Int. J. Heat Mass Transfer*, No. 47, 1141-1158.
- Oliveira P., F.T. Pinho, G.A. Pinto. 1998. "Numerical simulation of non-linear elastic flows with a general collocated finite-volume method." *Journal of Non-Newtonian Fluid Mechanics*, No. 79, 1-43.

Phan-Thien, N. and R. I. Tanner. 1977. "A new constitutive equation derived from network theory." *J. Non-Newtonian Fluid Mech*, No. 2 353-365.

Pinho, FT and P. J. Oliveira. 2001. "A metodologia dos volumes finitos aplicada à reologia computacional I: Introdução." *e-rheo.pt*, No. 1, 1-15.

Potente H., H. Ridder and R.V. Cunha. 2002. "Global concept for describing and investigation of wall slip effects in the extrusion process". *Macromolecular Materials and Engineering*. No. 11, 836-842.

Polyflow manual (implementation of boundary conditions).

Schowalter W. R. 1988. "The Behavior of Complex Fluids at Solid Boundaries." *J. Non-Newtonian Fluid Mech.*, No. 29, 25-36.

AUTHOR BIOGRAPHIES

LUIS L. FERRÁS studied Mathematics at the University of Aveiro and obtained his degree in 2005. In 2007 he obtained a master degree in Applied Mathematics from the Faculty of Science - University of Porto. He started in 2008 his PhD in Polymer Engineering- University of Minho.

JOÃO M. NÓBREGA studied Mechanical Engineering in the University of Porto and obtained his degree in 1994. In 1997 he obtained the master degree in Mechanical Engineering from the University of Porto. In 2004 he obtained his PhD in Polymer Engineering and Science from the University of Minho. He is now assistant professor at the University of Minho.

FERNANDO T. PINHO obtained in 1984 his degree in Mechanical Engineering from the Department of Mechanical Engineering at the University of Porto. In 1987 he obtained the Master of Science on "Thermal Engineering" from the Department of Mechanical Engineering at the University of Porto. In 1990 the PhD from the University of London (Imperial College of Science, Technology and Medicine). He is now Associate Professor at the University of Porto.

OLGA S. CARNEIRO obtained her degree in Production Engineering (Polymers) in 1985 and the PhD in 1994, in Polymer Engineering and Science, both from the University of Minho. She is now an Associate Professor at the Department of Polymer Engineering in the University of Minho.